Internal stress distribution in glass-covered amorphous magnetic wires

H. Chiriac, T. A. Óvári, and Gh. Pop

Institute of Technical Physics, 47 Mangeron Boulevard, 6600 Iaşi 3, Romania

(Received 10 February 1995; revised manuscript received 19 May 1995)

During the preparation process of the glass-covered magnetic amorphous wires, axial, radial, and azimuthal internal stresses are induced, determining their magnetic properties. We have proposed a calculation method of the internal stresses induced during the solidification of the metal and during the cooling from the solidification temperature to room temperature due to the difference between the thermal expansion coefficients of metal and glass. For $Fe_{77.5}Si_{7.5}B_{15}$ glass-covered amorphous wires we found internal stresses of about 10^9 Pa. The values and distribution of these stresses depend on the radius of the metal and on the thickness of the glass cover. The stress distribution coupled with the specific high positive magnetostriction leads to an easy axes distribution associated with a magnetic domain structure consisting of a cylindrical inner core with axial magnetization and a cylindrical outer shell with radial magnetization. The inner core leads to the appearance of a large Barkhausen jump at low axial fields. We have calculated the ratio M_r/M_s (the reduced remanence) as being of about 0.75–0.80. Magnetic measurements performed on samples prepared by us confirm the existence of the large Barkhausen jump but with a reduced remanence of about 0.95 that suggests the existence of a supplementary axial tensile stress. The dependence of the reduced remanence on external tensile stresses for wires covered by glass and after the glass removal confirms the existence of the supplementary stress whose value was estimated as being of the order of 10^8 Pa.

I. INTRODUCTION

Magnetic amorphous wires prepared by rapid quenching from the melt present a special interest for basic research as well as for their potential applications.[1-3] Metallic amorphous wires with diameters ranging between 80 and 160 μm are obtained using the in-water quenching technique.[1-5] The magnetic properties of these wires are related to the local anisotropy distribution produced by the magnetoelastic effects. The wire-shaped highly positive magnetostrictive amorphous alloys present a large Barkhausen jump at low axially applied magnetic fields.[6] The value of the remanent magnetization is approximately 0.5 of the saturation magnetization.[7] This magnetic bistability is caused by the magnetic domain structure that consists in two regions: an inner core with the easy axis parallel to the wire axis and an outer shell with radial easy axes.[8] It is generally accepted that this domain structure is due to the internal stresses induced during the solidification process.[9] This hypothesis is based on the calculation of the internal stresses,[10-13] as well as on the study of the magnetic properties of the wires subjected to external tensile stresses.

Some results were recently published on the magnetic properties of glass-covered amorphous wires prepared by rapid quenching from the melt[14] using an improved variant of the Taylor method that is presently known as the glass-coated melt spinning method.[15] This variant consists in the rapid drawing of a glass capillary in which the molten metal jet is entrapped; the metallic melt that is in the softened glass cover is ultrarapidly cooled by using a water jet. The metal is induction melted and the glass becomes soft being in contact with the molten alloy. By this method they found metallic amorphous wires covered by glass with diameters of the metallic part ranging between 3 and 25 μm and with the thickness of the glass cover ranging between 2 and 15 μm. This kind of wires, prepared from highly positive magnetostrictive alloys, also presents a large Barkhausen effect at low axial fields. These glass-covered amorphous wires attract remarkable interest because they have very small dimensions as compared to those of the amorphous wires prepared by the in-rotating-water spinning method, and offer the possibility of studying the direct and indirect influence of the glass cover on the physical properties of these wires by preparing samples with different values of the glass cover thickness for the same diameter of the wire's metallic part. The magnetic properties of these wires are related to the mechanical stresses induced during their fabrication. These stresses are much more complex in the case of glass-covered wires than in the case of the wires without glass covers prepared by the in-water quenching technique because in the first case the internal stresses come from the glass transition process of the metal as well as from the constraints produced on the metal by the cooled glass cover as a result of the difference between the thermal expansion coefficients of the two materials and also from the preparation process through the axial tension continuously applied on the wire.

The aim of this paper is the evaluation of the internal stresses induced during the preparation of glass-covered amorphous wires including the calculation of their distribution in the function of the wire's dimensional characteristics and the study of the influence of these dimen-

sional characteristics on the stress distribution. Magnetic measurements were performed in order to verify the results obtained by theoretical considerations.

II. CALCULATION OF INTERNAL STRESS DISTRIBUTION

We consider that the preparation process of the glass-covered amorphous metallic wires has two separate stages, accomplished in successive time and temperature intervals. The first stage is the glass transition of the metal that, for simplicity, is assumed to take place simultaneously with the hardening of the glass at the glass transition temperature T_g. In the approach we have taken, we assumed that the glass transition phenomenon is a simple solidification process. The second stage is the cooling of the metal-glass ensemble from T_g to room temperature (RT). In the first stage, internal stresses are induced due to the solidification of the metal as the solidification front proceeds radially inward to the center of the wire. In the second stage, internal stresses are induced due to the contraction of the two materials (metal and glass) having different thermal expansion coefficients. In addition, there is an axial tensile stress continuously applied on the wire due to its drawing during the preparation process. We will now calculate the internal stress distribution for the particular case of a $Fe_{77.5}Si_{7.5}B_{15}$ glass-covered wire. The glass transition temperature for the $Fe_{77.5}Si_{7.5}B_{15}$ alloy is assumed to be approximately 1000 K.

A. Internal stresses induced during the solidification of the metal

We calculate the internal stress distribution induced due to the solidification of the metal in cylindrical coordinates that are the most appropriate in this problem due to its symmetry. Figure 1 illustrates the diagonal components of the stress tensor σ (σ_{rr}, $\sigma_{\theta\theta}$, and σ_{zz}) induced in the infinitesimal element of volume dV that is centered on the point $P(r)$, r being an arbitrary selected point on the radius. We assume that the other components of σ are null.

We can consider that the metallic cylinder consists of successive concentric cylindrical shells, each shell having a thickness of dr. These shells are solidifying consecutively starting from outside due to the temperature gradient at the glass transition temperature $(dT/dr)_{T=T_g}$. Due to the very small radial dimensions involved in this process, we can consider that the decisive role in the rapid solidification process is played by the temperature gradient on the radial direction. In order to calculate the value of the temperature gradient in each shell we must find the radial and time dependencies of the temperature in the wire (metal+glass). With this aim we solve the differential equation of the temperature field considering that the heat transfer takes place only by conduction, the other types of heat transfer being neglected. Considering temperature-independent properties for both materials, the temperature field equation in cylindrical coordinates is[16]
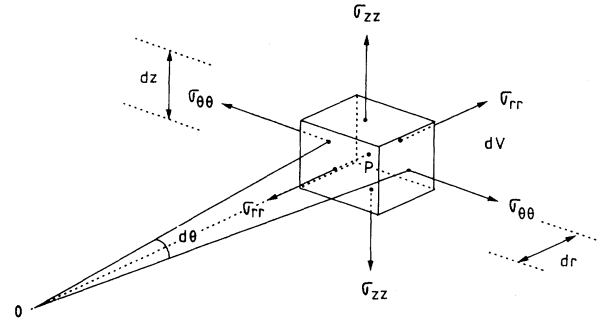

FIG. 1. Diagonal stress components corresponding to the infinitesimal element of volume dV centered on $P(r)$, that is found in the metallic part of the wire, represented in the cylindrical system of coordinates with the z axis parallel to the longitudinal axis of the wire.

$$\frac{\partial T}{\partial t} = \frac{D}{r}\frac{\partial}{\partial r}\left[r\frac{\partial T}{\partial r}\right] = D\left[\frac{\partial^2 T}{\partial r^2} + \frac{1}{r}\frac{\partial T}{\partial r}\right], \quad (1)$$

where $T = T(r,t)$ is the temperature in the point r on the radius at any instant t, r is the radial coordinate, t is the instant of time, $D = k/\rho c$ is the thermal diffusivity, k is the thermal conductivity, c is the specific heat and ρ is the density.

We solve (1) separately for the glass cover and for the metallic part of the wire by imposing the following conditions: for the metal,

$$T(r=0, t=0) = T_m$$

and

$$T(r=R_m, t)_{|\text{metal}} = T(r=R_m, t)_{|\text{glass}} ;$$

for the glass cover,

$$T(r=R_m, t=0) = T_m$$

and

$$T(r=R_w, t=0) = T_w ,$$

where R_m is the radius of the metallic part of the wire, R_w is the radius of the glass-covered wire, T_m is the melting temperature, and T_w is the temperature of the cooling agent (water).

The solution of Eq. (1) is in this case

$$T(r,t) = T_w + (T_m - T_w)\sum_{j=1}^{\infty}\frac{2}{\beta_j J_1(\beta_j)}J_0\left[\beta_j\frac{r}{R_w}\right]$$

$$\times \exp\left[-\frac{D\beta_j^2}{R_w^2}t\right], \quad (2)$$

in which β_j's are the roots of the equation $J_0(\beta)=0$ and J_0, J_1 are the zero- and first-order Bessel functions.

For a $Fe_{77.5}Si_{7.5}B_{15}$ metallic wire, prepared in a Pyrex glass cover, having $R_m = 3.65$ μm, the thickness of the glass cover (d_g) of 7.50 μm, $R_w = 11.15$ μm, $\rho = 7200$
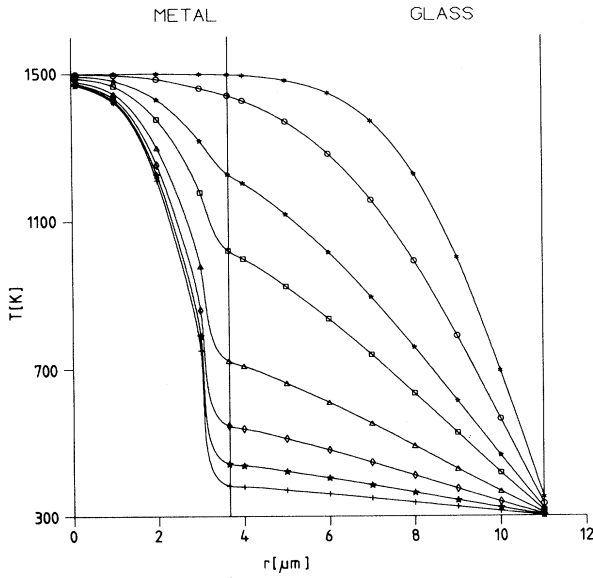
FIG. 2. Radial temperature distributions in the wire after 5 μs (∗), 10 μs (○), 20 μs (★), 30 μs (□), 50 μs (△), 70 μs (◇), 90 μs (☆), and 110 μs (+) from the start of the rapid solidification process.

kg/m^3, $c = 530$ J/kg K, $k = 30$ W/mK, $T_m = 1500$ K, and $T_w = 300$ K, the radial distribution of temperature at different instants of time is illustrated in Fig. 2. For the Pyrex glass the following parameters were considered: $\rho = 2413$ kg/m^3, $c = 837$ J/kg K, and $k = 1.177$ W/mK. An abrupt change in the slope of the $T(r)$ curves is observed at the metal-glass interface.

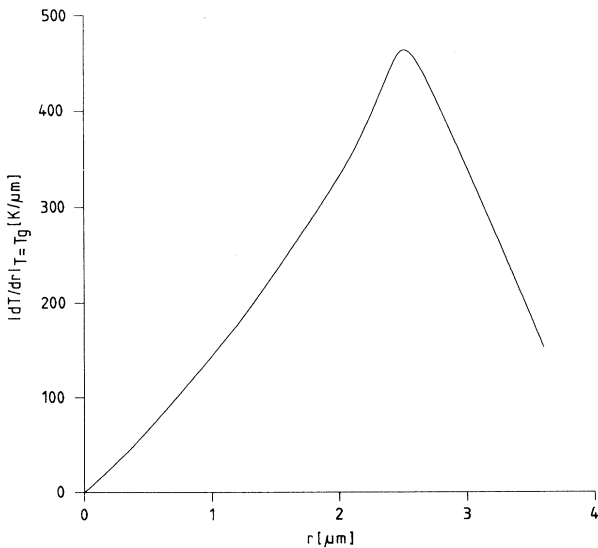Starting from the curves $T(r)$ at different instants of time t, we can determine the radial dependence of the

temperature gradient at the glass transition temperature (which is assumed to be the solidification temperature): $(dT/dr)_{T=T_g} = f(r)$. This dependence is necessary in order to calculate the internal stresses. The curve $|dT/dr|_{T=T_g}(r)$ is shown in Fig. 3.

We consider a small cylindrical shell of thickness dr, ranging between the inner radius x and the outer radius $x + dr$, which solidifies due to the temperature gradient $(dT/dr)_{T=T_g}$ that corresponds to this shell which is associated to the point $r = x$ and whose value can be determined from the curve illustrated in Fig. 3. The stress components induced due to the solidification of the considered shell are given by[17]

$$\sigma_{rr}(r,x) = \frac{\alpha_m E_m}{1-\nu} \frac{1}{r^2}$$
$$\times \left[\frac{r^2-x^2}{R_m^2-x^2} \int_x^{R_m} T(r)r\,dr - \int_x^r T(r)r\,dr \right], \tag{3}$$

$$\sigma_{\theta\theta}(r,x) = \frac{\alpha_m E_m}{1-\nu} \frac{1}{r^2}$$
$$\times \left[\frac{r^2+x^2}{R_m^2-x^2} \int_x^{R_m} T(r)r\,dr + \int_x^r T(r)r\,dr \right.$$
$$\left. - T(r)r^2 \right], \tag{4}$$

$$\sigma_{zz}(r,x) = \frac{\alpha_m E_m}{1-\nu} \left[\frac{2}{R_m^2-x^2} \int_x^{R_m} T(r)r\,dr - T(r) \right], \tag{5}$$

FIG. 3. Radial distribution of the temperature gradient at the solidification temperature (1000 K) in the metallic part of the wire.
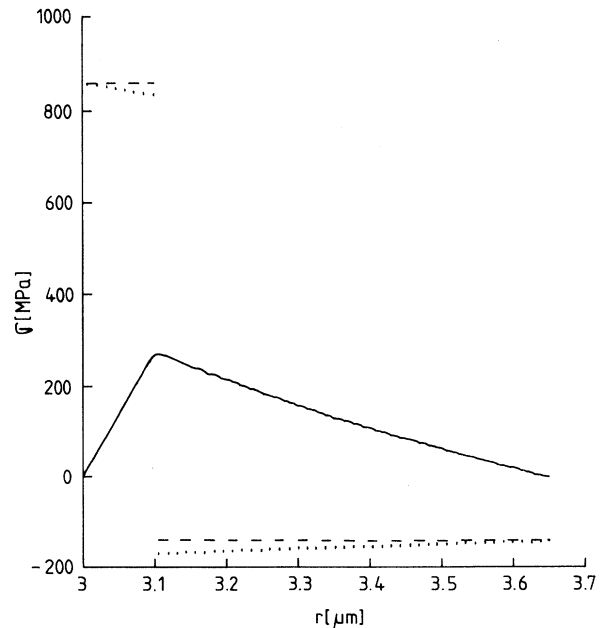

FIG. 4. Radial distribution of the stresses induced during the solidification of the cylindrical shell that ranges between $x = 3.0$ μm and $x + dr = 3.1$ μm; σ_{rr} (solid line), $\sigma_{\theta\theta}$ (dotted line), and σ_{zz} (dashed line).

where $\nu = 0.33$ is Poisson's coefficient, $E_m = 2 \times 10^{11}$ N/m² is Young's modulus, and $\alpha_m = 8.7 \times 10^{-6}$ K^{-1} is the thermal expansion coefficient of the metal.

By the correspondence $\sigma_{ii}(r)$ we understand the stress component induced in the direction i in the infinitesimal element of volume dV that is centered on the point r on the radius. If we choose the infinitesimal element of length on the radius dr used in order to calculate the temperature gradient equal to the thickness of the considered cylindrical shell $dr = 0.1$ μm, then $T(r)$ from relations (3)–(5) is exactly the temperature gradient. In (3)–(5), r takes values from x to R_m. In order to calculate the stresses induced due to the solidification of the cylindrical shell having r ranging between x and $x + dr$ in the entire interval $[x, R_m]$, we will consider the following temperature distribution in this interval:

$$T(r) = - \left| \frac{dT}{dr} \right|_{T=T_g} (r), \quad x \leq r \leq x + dr \text{ and } 0 \text{ in rest },$$

(6)

where $|dT/dr|_{T=T_g}$ is determined from the graph shown in Fig. 3. This approximation is quite plausible because the solidification of the considered shell has no effect on the part between $r = 0$ and $r = x$, this part being still liquid, and the part between $r = x + dr$ and $r = R_m$ is already solidified so we can consider that in this region the temperature gradient is null.

Using relations (3)–(6) we have calculated the internal stress distribution due to the solidification of the cylindrical shell ranging between $x = 3.0$ μm and $x + dr = 3.1$ μm for the considered wire. This distribution is illustrated in Fig. 4. Due to the temperature distribution (6) considered above, σ_{zz} and $\sigma_{\theta\theta}$ present a discontinuity at the interface between the already solidified metal and the currently solidifying shell. A physical interpretation of this discontinuity is that the inner shell tries to shrink be-
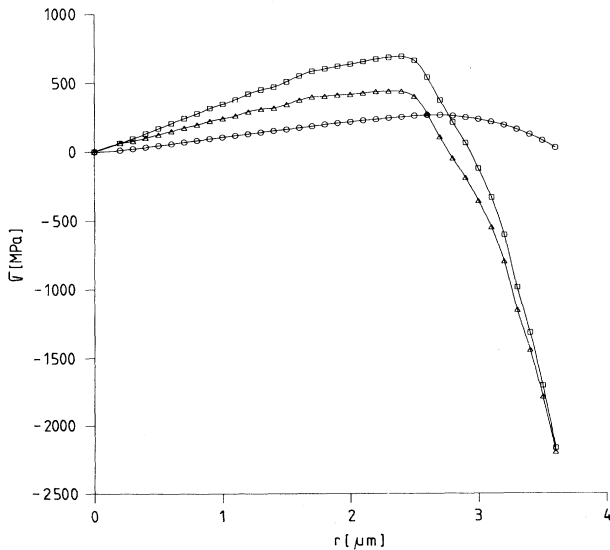
ing subjected to a tensile opposition from the outer one which simultaneously feels a compression. The final stress distribution in the metallic part of the wire, generated by its solidification, has been calculated by adding the local distributions obtained after the successive solidification of each metallic shell having the thickness dr. The final solidification stress distribution for the considered wire is illustrated in Fig. 5.

B. Stresses induced during the cooling from T_g to RT due to the difference between the thermal expansion coefficients of the metal and glass

The cooling from T_g to RT is a slow process as compared to the rapid in-water quenching that takes place in the T_m-T_g interval. For this reason, for the calculation of the stresses induced during the cooling from T_g to RT we will neglect in the followings the radial dependence of the temperature $T(r)$. We consider that the components of the displacement vector $\mathbf{u}$ of any point of the wire, namely u_r, u_θ, and u_z are independent one of the others. Due to the symmetry of the cooling process and implicitly of the displacements and strains generated by this process, we have $u_\theta = $const in the metal as well as in the glass. In these hypotheses, $\Delta \times \mathbf{u} = 0$, and the equilibrium equation of $\mathbf{u}$ is[18]

$$\text{grad div} \mathbf{u} = 0 .$$

(7)

Equation (7) implies

$$\text{div} \mathbf{u} = \text{const} .$$

(8)

For simplicity, we consider that the values of Poisson's coefficient for metal and glass are the same: $\nu_{\text{metal}} = \nu_{\text{glass}} = \nu = \frac{1}{3} = 0.33$.

Equation (8) contains three equations, one after each direction; r, θ, and z. Thus, we have to solve just the following two equations:

$$-r: \quad \frac{du_r}{dr} + \frac{u_r}{r} = \text{const} ,$$

(9)

$$-z: \quad \frac{du_z}{dz} = \text{const}$$

(10)

We can set const$=2a$ in (9) and const$=b$ in (10). The general solution of equation (9) will now be

$$u_r(r) = ar + \frac{c}{r} ,$$

(11)

in which c is an integration constant.

We notice that in the center of the wire (at $r = 0$), due to the symmetry of the process, there is actually no radial displacement. This implies the following condition:

$$u_r^m(0) = 0 ,$$

(12)

where u_r^m is the radial displacement in the metal. The condition (12) is accomplished according to (11) just when the constant c is zero in the metal. Thus, the solutions (11) that give us the radial displacements are in the metal,

$$u_r^m(r) = a_m r ,$$

(13)

FIG. 5. Final radial stress distribution in the metal due to its solidification: $\sigma_{rr}(\bigcirc)$, $\sigma_{\theta\theta}(\triangle)$, and $\sigma_{zz}(\square)$.

and in the glass,

$$u_r^g(r) = a_g r + \frac{c}{r} , \qquad (14)$$

where u_r^g is the radial displacement in the glass, a_m and a_g are the constants a from (11) for metal and glass, respectively, and c is the integration constant from (11) for the glass.

The solutions for the axial displacements are determined by integration from (10): in the metal,

$$u_z^m(z) = b_m z , \qquad (15)$$

and in the glass,

$$u_z^g(z) = b_g z , \qquad (16)$$

where u_z^m, u_z^g are the axial displacements in the metal and glass respectively and b_m, b_g are the constants b for metal and glass, respectively.

The components of the strain tensor can be detected from the displacements given by (13)–(16) and from the azimuthal displacements $u_\theta^m = $const and $u_\theta^g = $const. The diagonal components of the strain tensor, assuming that the other components are null, are for the metal,

$$u_{rr}^m = \frac{du_r^m}{dr} = a_m ,$$

$$u_{\theta\theta}^m = \frac{1}{r}\frac{du_\theta^m}{d\theta} + \frac{u_r^m}{r} = a_m , \qquad (17)$$

$$u_{zz}^m = \frac{du_z^m}{dz} = b_m ,$$

and for the glass cover,

$$u_{rr}^g = \frac{du_r^g}{dr} = a_g - \frac{c}{r^2} ,$$

$$u_{\theta\theta}^g = \frac{1}{r}\frac{du_\theta^g}{d\theta} + \frac{u_r^g}{r} = a_g + \frac{c}{r^2} , \qquad (18)$$

$$u_{zz}^g = \frac{du_z^g}{dz} = b_g ,$$

in which u_{rr}^m, $u_{\theta\theta}^m$, and u_{zz}^m are the radial, azimuthal, and axial strains in the metal and u_{rr}^g, $u_{\theta\theta}^g$, and u_{zz}^g are the same strain components in the glass. It is necessary to make an observation here: the range in which the radial coordinate r takes values is $(0, R_m]$ for the strains that appear in the metal and $(R_m, R_w]$ for those that appear in the glass. The reason why the expressions (17) cannot be defined in $r = 0$ is that $u_{\theta\theta}^m$ would be ∞ in this case.

We substitute the strain tensor components given by (17) and (18) in Hooke's law in order to calculate the diagonal components of the stress tensor. Considering the simplest case of homogeneous strains, Hooke's law gives[18]

$$\sigma_{ik} = \frac{E}{1+v}\left[u_{ik} + \frac{v}{1-2v} u_{ll}\delta_{ik} \right] , \qquad (19)$$

where E is Young's modulus, u_{ik} are the components of

the strain tensor, σ_{ik} are the components of the stress tensor, and δ_{ik} is the Kronecker symbol.

Particularizing (19) for the diagonal components of the stress tensor, we obtain

$$\sigma_{rr} = \frac{E}{(1+v)(1-2v)}[(1-v)u_{rr} + v(u_{\theta\theta} + u_{zz})] ,$$

$$\sigma_{\theta\theta} = \frac{E}{(1+v)(1-2v)}[(1-v)u_{\theta\theta} + v(u_{rr} + u_{zz})] , \qquad (20)$$

$$\sigma_{zz} = \frac{E}{(1+v)(1-2v)}[(1-v)u_{zz} + v(u_{rr} + u_{\theta\theta})] .$$

By taking into account (17) and (18), (20) becomes for the metal,

$$\sigma_{rr}^m = \frac{E_m}{(1+v)(1-2v)}(a_m + v b_m) ,$$

$$\sigma_{\theta\theta}^m = \frac{E_m}{(1+v)(1-2v)}(a_m + v b_m) , \qquad (21)$$

$$\sigma_{zz}^m = \frac{2E_m v}{(1+v)(1-2v)}(a_m + v b_m) + E_m b_m ,$$

and for the glass,

$$\sigma_{rr}^g = \frac{E_g}{(1+v)(1-2v)}(a_g + v b_g) - \frac{E_g}{1+v}\frac{c}{r^2} ,$$

$$\sigma_{\theta\theta}^g = \frac{E_g}{(1+v)(1-2v)}(a_g + v b_g) + \frac{E_g}{1+v}\frac{c}{r^2} , \qquad (22)$$

$$\sigma_{zz}^g = \frac{2E_g v}{(1+v)(1-2v)}(a_g + v b_g) + E_g b_g ,$$

E_m and E_g being Young's modulus for the metal and for the glass, respectively.

We will now calculate the resultant strain due to the cooling of two materials with different thermal expansion coefficients which are in contact during the entire process. The law of the linear thermal expansion is

$$l = l_0(1 + \alpha\Delta T) , \qquad (23)$$

in which l is the linear dimension of the body in the chosen direction at the temperature T, l_0 is the same linear dimension at the temperature T_0, $\Delta T = T - T_0$ is the temperature range in which the variation $\Delta l = l - l_0$ takes place, and α is the thermal expansion coefficient. From (23) we have for the metal

$$\varepsilon_m = \alpha_m \Delta T , \qquad (24)$$

and for the glass

$$\varepsilon_g = \alpha_g \Delta T , \qquad (25)$$

where ε_m, ε_g are the strains due to the thermal contraction in the metal and glass respectively and α_m, α_g are the thermal expansion coefficients of the metal and glass. The resultant strain will be

$$\varepsilon = \varepsilon_m - \varepsilon_g = (\alpha_m - \alpha_g)\Delta T . \qquad (26)$$

In this case, ΔT is the difference between the glass transition temperature and the room temperature, be-

cause, from the point of view of the stresses induced due to the difference in thermal expansion coefficients, this is the determinate temperature range in which the thermal contraction takes place.

In order to determine σ_{rr}^m, $\sigma_{\theta\theta}^m$, and σ_{zz}^m we must find the values of the constants a_m and b_m. With this aim, we will establish the equilibrium conditions, including those at the metal-glass interface. But first of all we have to impose the following conditions so that all the strains that appear in this process result due only to the difference between the thermal expansion coefficients of the metal and glass:

$$u_z^m(r=R_m)-u_z^g(r=R_m)=\varepsilon z \ , \tag{27}$$

$$u_r^m(r=R_m)-u_r^g(r=R_m)=\varepsilon R_m \ . \tag{28}$$

In (27) and (28) we have maintained the hypothesis of the homogeneous strains.

The equilibrium conditions are

$$F_r^{\text{res}}(r=R_w)=0 \ , \tag{29}$$

$$F_r^{\text{res}}(r=R_m)=0 \ , \tag{30}$$

$$F_z^{\text{res}}(r=R_m)=0 \ , \tag{31}$$

in which F^{res} is the resultant force on the indicated direction. Explicitly, after several transformations, (29), (30), and (31) become

$$F_r^{\text{res}}(r=R_w)=0 \Longleftrightarrow \sigma_{rr}^g(r=R_w)=0 \ , \tag{32}$$

$$F_r^{\text{res}}(r=R_m)=0 \Longleftrightarrow \sigma_{rr}^m(r=R_m)-\sigma_{rr}^g(r=R_m)=0 \ , \tag{33}$$

$$F_z^{\text{res}}(r=R_m)=0 \Longleftrightarrow \sigma_{zz}^m(r=R_m)+S\sigma_{zz}^g(r=R_m)=0 \ , \tag{34}$$

where $S=S_{\text{tr}}^g/S_{\text{tr}}^m$; S_{tr}^g and S_{tr}^m being the cross section areas of the glass cover and of the metallic wire, respectively.

Using (13)–(16) and (21)–(22), the conditions (27), (28), (32), (33), and (34) will constitute the following system of equations:

$$b_m-b_g=\varepsilon \ ,$$

$$a_m R_m - a_g R_m - \frac{c}{R_m}=\varepsilon R_m \ ,$$

$$\lambda_g\left[a_g+vb_g-(1-2v)\frac{c}{R_w^2}\right]=0 \ , \tag{35}$$

$$\lambda_m(a_m+vb_m)-\lambda_g\left[a_g+vb_g-(1-2v)\frac{c}{R_m^2}\right]=0 \ ,$$

$$2\lambda_m v(a_m+vb_m)+E_m b_m$$
$$+S[2\lambda_g v(a_g+vb_g)+E_g b_g]=0 \ ,$$

in which we denominated $\lambda_m=E_m/(1+v)(1-2v)$ and $\lambda_g=E_g/(1+v)(1-2v)$. For the considered particular case we have $R_w=11.15$ μm and $R_m=3.65$ μm, from which it results that $S=8.33$.

Solving the algebraic system (35) for the unknown

quantities a_m, b_m, a_g, b_g, and c with the parameters $E_m=2\times10^{11}$ N/m^2, $E_g=10^{11}$ N/m^2, $v=\frac{1}{3}$, and $\varepsilon=3.78\times10^{-3}$ [from (26) with $\alpha_m=8.7\times10^{-6}$ K^{-1} and $\alpha_g=3.3\times10^{-6}$ K^{-1}], we found for a_m and b_m [which are necessary in (21)] the following expressions:

$$a_m=\varepsilon\psi S\frac{\psi S-S}{[(\psi+3)S+4](\psi S+1)} \ , \tag{36}$$

$$b_m=\frac{\varepsilon\psi S}{\psi S+1} \ , \tag{37}$$

where by ψ we denominated the ratio E_g/E_m.

Substituting (36) and (37) in (21) we obtained the expressions of the internal stresses induced in the cooling from T_g to RT due to the difference between the thermal expansion coefficients of metal and glass:

$$\sigma_{rr}^m=\sigma_{\theta\theta}^m=\frac{3\psi S}{(\psi+3)S+4}\varepsilon E_m \ , \tag{38}$$

$$\sigma_{zz}^m=\sigma_{rr}^m\frac{(\psi+1)S+2}{\psi S+1} \ . \tag{39}$$

In the particular case we have referred to, the value of these stresses are

$$\sigma_{rr}^m=\sigma_{\theta\theta}^m=287.28 \text{ MPa}; \quad \sigma_{zz}^m=807.26 \text{ MPa} \ .$$

We notice here that these stresses do not depend on the coordinates (r,θ,z) in the range $(0,R_m]$. The center of the wire $(r=0)$ constitutes a singularity in which all the stress components must be null in order to ensure the equilibrium in this point.

C. Total stresses induced during the preparation of the glass covered amorphous wires. Results and discussion

The total stresses are calculated by adding the different stress components induced in the two considered stages of the preparation process. Thus, we will add the stresses induced in the solidification process to those induced in the slow cooling from T_g to RT due to the difference between the thermal expansion coefficients of metal and glass. For the moment we neglect the axial tensile stress generated by the continuous drawing specific to this kind of preparation process. The total stress distribution in this particular case is illustrated in Fig. 6. We notice that the radial dependence of the temperature in the glass influences the cooling of the metal and this influence can be observed in Fig. 4. Thus, the radial distribution of the temperature in the glass influences the internal stresses through the temperature gradient in the metal. One observes that the shape of the curves $\sigma_{zz}(r)$ and $\sigma_{\theta\theta}(r)$ is the same, but the positive values of $\sigma_{zz}(r)$ are almost twice the positive values of $\sigma_{\theta\theta}(r)$. Both curves present a positive maximum value at $r=2.4$ μm: $\sigma_{zz}(2.4\mu\text{m})$ ~1500 MPa and $\sigma_{\theta\theta}(2.4\mu\text{m})$ ~730 MPa. After reaching the maximum, both $\sigma_{zz}(r)$ and $\sigma_{\theta\theta}(r)$ decrease drastically, reaching near the surface of the metal high negative values: $\sigma_{zz}(3.6\mu\text{m})$ ~ −1360 MPa and $\sigma_{\theta\theta}(3.6\mu\text{m})$ ~ −1910 MPa $\sigma_{rr}(r)$ has a much moderate variation than $\sigma_{zz}(r)$ and $\sigma_{\theta\theta}(r)$, having only positive values.
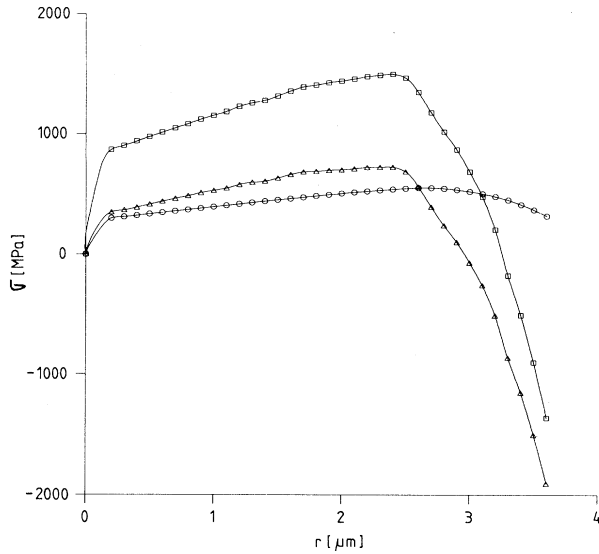
FIG. 6. Total stress distribution (solidification stresses added to those induced due to the difference between the thermal expansion coefficients of metal and glass) in the metallic part of the wire: σ_{rr} ($\bigcirc$), $\sigma_{\theta\theta}$ ($\triangle$), and σ_{zz} ($\square$).

Thus, the radial stresses are tensile everywhere in the range $(0, R_m)$, while the axial and azimuthal ones are tensile from $r = 0$ to approximately 82% of R_m, changing sign close to the surface where they become compressive. The curve $\sigma_{rr}(r)$ reaches a maximum value at $r = 2.7 \ \mu m$ of ~ 550 MPa after which it decreases having a slope with an absolute value higher than that of the ascendant portion of the curve (till it reaches the maximum value). We mention that $\sigma_{zz}(r)$ and $\sigma_{\theta\theta}(r)$ do not intersect each other, both being intersected by $\sigma_{rr}(r)$. The intersection point between $\sigma_{zz}(r)$ and $\sigma_{rr}(r)$ is at $\sim 85\%$ of R_m. Starting from the center of the wire up to this point we have a region in which σ_{zz} is the component with the highest value and it is positive (zone I). From $\sim 85\%$ of R_m to $\sim 88\%$ of R_m we have a second region, much narrower than the first one, in which σ_{rr} is the highest stress component and it is positive (zone II). The remaining part up to R_m constitutes a third region, dominated by the high negative values (compression) of σ_{zz} and $\sigma_{\theta\theta}$ (zone III). The values of the internal stresses on each direction and the position of the intersection point between the radial and axial stresses with respect to the dimension of the metallic part of the wire determine the dimensions of these three zones.

By taking into account the fact that the alloy to which we referred is highly magnetostrictive, there will appear a strong coupling between the internal stresses and the magnetostriction.[19] Due to this coupling, in the metallic part of the wire there will form easy axes of magnetization on the directions in which the dominant internal stresses are tensile (positive) and hard axes on the directions in which the dominant stresses are compressive

(negative). Thus, on the grounds of magnetoelastic energy minimization, we can consider that in the metallic part of the wire, starting from its center, we will have three zones, namely, (i) zone I with a uniaxial magnetic anisotropy having the easy axis oriented along the axis of the wire (z axis) due to the coupling between σ_{zz} (positive) and the magnetostriction; (ii) zone II with a radial magnetic anisotropy due to the coupling between σ_{rr} (positive) and the magnetostriction; (iii) zone III with two strongly compressive components (σ_{zz} and $\sigma_{\theta\theta}$), which are comparable by magnitude and have absolute values much higher than σ_{rr}. These compressive stress components generate two hard axes of magnetization on the axial and azimuthal directions. Thus, in this zone we will

FIG. 7. (a) Maximum value of the total axial stress in function of the radius of the metal for three wires having almost the same glass cover thickness: wire Nos. 4 ($\blacksquare$), 5 ($\square$) and, 6 ($\blacksquare$) from Table I; (b) Position of the relative intersection point between σ_{rr} and σ_{zz} in function of the radius of the metal for wire Nos. 4 ($\blacksquare$), 5 ($\square$), and 6 ($\blacksquare$).

also have an easy axis of magnetization on the radial direction that is energetically favored by the coupling between the magnetostriction and σ_{rr} (positive).
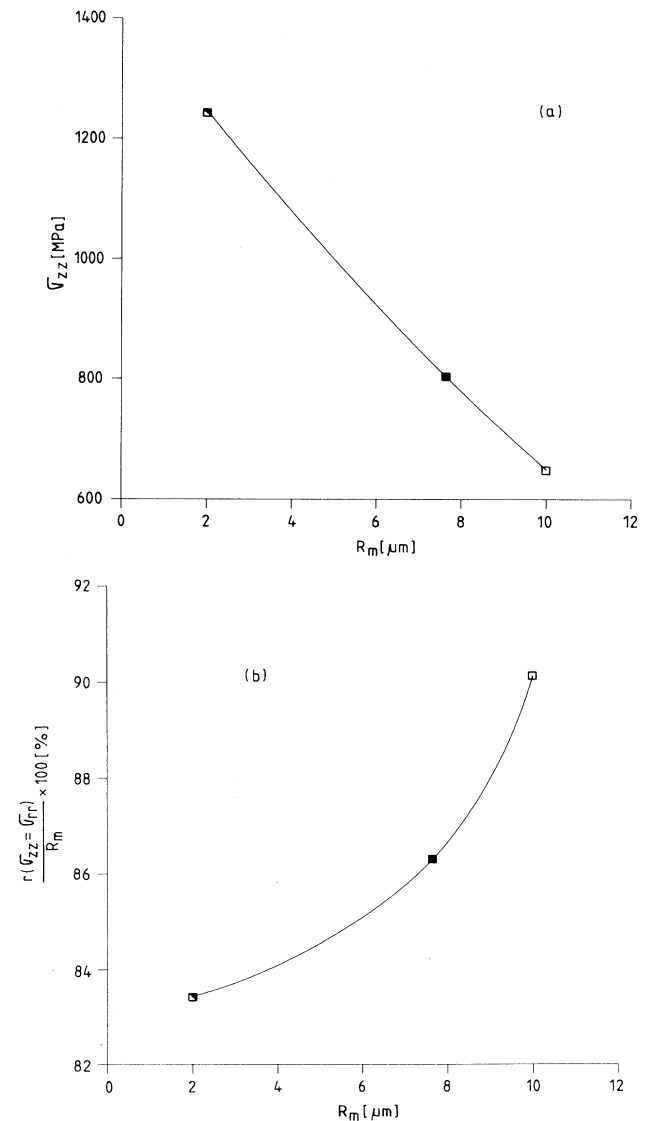
By taking into account the above-mentioned discussions, it can be considered by analogy with the case of the wires prepared by the in-rotating-water spinning method,[20] that for the glass-covered magnetic amorphous wires prepared from a highly positive magnetostrictive alloy there will result a magnetic domain structure consisting of two regions: a cylindrical inner core having an axial easy axis ad an outer shell having radial easy axes. For the considered case, the radius of the cylindrical inner core (R_c) is approximately 85% of R_m.

The considered domain structure depends on the distribution of the total internal stresses that appear in the preparation process of the wire and which, in turn, strongly depends on the diameter of the metallic part of the wire and on the thickness of the glass cover, as well as on their ratio.

Using the above described method, we calculated the internal stress distribution for six glass-covered wires, considered as being representative cases. The dimensional characteristics of these wires are listed in Table I, together with the maximum positive values of the three stress components induced in each stage of the preparation process and the maximum positive values of the total stresses in each direction, as well as the maximum negative values of σ_{zz} and $\sigma_{\theta\theta}$ induced in the solidification process and the same values for the total axial and azimuthal stress components. The maximum negative values of σ_{zz} and $\sigma_{\theta\theta}$ were calculated in points situated very close to the surface of the metal in each considered case. In Table I, the positions of the intersection points between $\sigma_{zz}(r)$ and $\sigma_{rr}(r)$ for each wire are also listed.

In order to analyze the influence of the metal's dimen-

sion on the internal stress distribution, we represented in Fig. 7(a) the maximum value of the total axial stress in function of R_m for three wires having approximately the same thickness of the glass cover (wire Nos. 4–6 from Table I) and in Fig. 7(b) the position of the intersection point between $\sigma_{zz}(r)$ and $\sigma_{rr}(r)$ as a percentage of R_m in function of R_m for the same wires. It can be observed that the maximum value of σ_{zz} decreases almost linearly with the increase of R_m from 1250 MPa for $R_m=2$ μm (wire No. 6) to 650 MPa for $R_m=10$ μm (wire No. 5). From figure 7(b) one can observe that $r(\sigma_{zz}=\sigma_{rr})/R_m$ (the ratio between the intersection distance and the radius of the metal) increases with the increase of R_m from $\sim 83\%$ for wire No. 6 to $\sim 90\%$ for wire No. 5.

In order to analyze the influence of the glass cover's thickness (d_g) on the stress distribution, we represented in Fig. 8(a) the maximum value of the total axial stress in function of d_g for three wires having approximately the same R_m (wire Nos. 1, 2, and 6 from Table I) and in Fig. 8(b) the position of the intersection point between $s_{zz}(r)$ and $s_{rr}(r)$ as a percentage of R_m in function of d_g. From Fig. 8(a) it can be observed that the maximum value of σ_{zz} increases with the increase of d_g from 1250 MPa for $d_g=4.5$ μm (wire No. 6) to 1720 MPa for $d_g=15$ μm (wire No. 2). We notice that starting from $d_g \sim 10$ μm the maximum value of σ_{zz} is maintained approximately constant around the value of 1700 MPa when d_g increases. From Fig. 8(b) one can observe that the influence of d_g on the ratio $r(\sigma_{zz}=\sigma_{rr})/R_m$ is very reduced.

From the above presented data we observe that the internal stresses depend on the ratio d_g/R_m. In Fig. 9 the dependence of the ratio $r(\sigma_{zz}=\sigma_{rr})/R_m$ on the value of the ratio d_g/R_m for five wires (Nos. 1–6) from Table I is illustrated. Initially, one can observe a strong displace-

TABLE I. Maximum values of internal stresses for six selected samples of glass-covered wires.

Wire No.	Dimensional characteristics [μm]	Induced at the solidification of the metal					Induced at the cooling from T_g to RT		Total stresses					$r(\sigma_{rr}=\sigma_{zz})/R_m$ [%]
		σ_{rr}^{max}	σ_{zz}^{max}	$\sigma_{zz}^{surface}$	$\sigma_{\theta\theta}^{max}$	$\sigma_{\theta\theta}^{surface}$	$\sigma_{rr}=\sigma_{\theta\theta}$	σ_{zz}	σ_{rr}^{max}	σ_{zz}^{max}	$\sigma_{zz}^{surface}$	$\sigma_{\theta\theta}^{max}$	$\sigma_{\theta\theta}^{surface}$	
1	$\Phi_{metal}=5.00$ $d_{glass}=10.00$ $\Phi_{total}=25.00$	354	793	−1680	486	−1752	309	903	663	1696	−777	796	−1442	83.3
2	$\Phi_{metal}=5.00$ $d_{glass}=15.00$ $\Phi_{total}=35.00$	345	783	−1658	487	−1727	316	937	662	1720	−721	803	−1410	83.7
3	$\Phi_{metal}=7.30$ $d_{glass}=7.50$ $\Phi_{total}=22.30$	266	693	−2164	440	−2195	287	807	553	1500	−1357	727	−1907	84.6
4	$\Phi_{metal}=15.30$ $d_{glass}=4.75$ $\Phi_{total}=24.80$	133	338	−2047	212	−2089	190	465	323	803	−1582	402	−1899	86.3
5	$\Phi_{metal}=20.00$ $d_{glass}=5.00$ $\Phi_{total}=30.00$	100	245	−1516	159	−1592	170	404	270	649	−1112	328	−1423	90.1
6	$\Phi_{metal}=4.00$ $d_{glass}=4.50$ $\Phi_{total}=13.00$	188	443	−728	310	−934	286	804	474	1246	−150	596	−648	83.4

ment (from ~ 90 to ~ 83 % of R_m) of the intersection point (that determines the diameter of the cylindrical inner core) with the increase of the ratio d_g/R_m in a very narrow range of values (from 0.5 to 2.0) and starting from $d_g/R_m \sim 2.0$ the position of the intersection point remains practically constant (around 83% of R_m).

The results presented above show that by changing the dimensional parameters of the glass-covered amorphous wires (the radius of the metal, the thickness of the glass cover, and their ratio), one can obtain internal stress distributions that lead to the formation of a cylindrical inner cover with a uniaxial longitudinal anisotropy having a radius (R_c) that ranges between ~ 83 and ~ 90 % of R_m. This leads to the appearance of a large Barkhausen jump
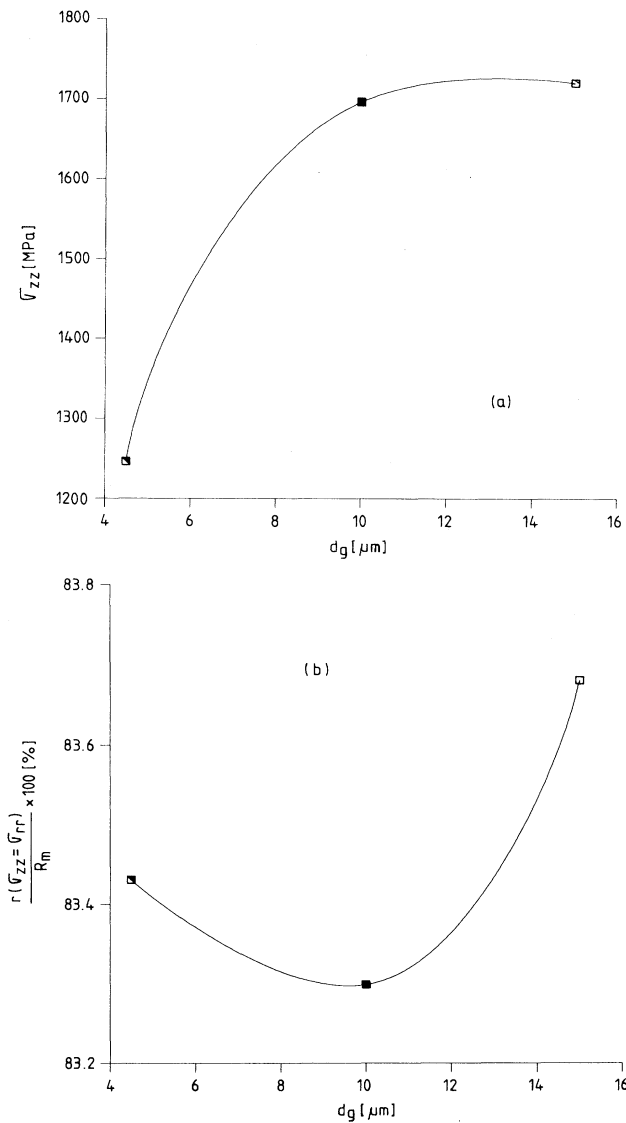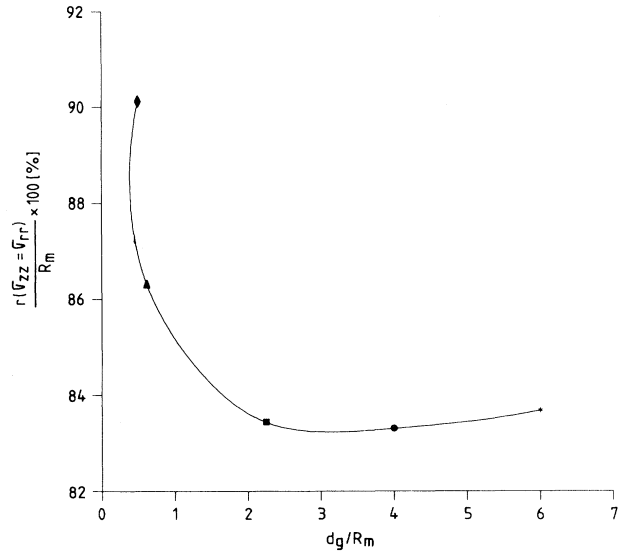
FIG. 9. Position of the relative intersection point between s_{rr} and s_{zz} in function of the ratio between the glass cover thickness and the radius of the metal for wire Nos. 1 (●), 2 (*), 4 (▲), 5 (♦), and 6 (■) from Table I.

in low axially applied magnetic fields so that the value of the remanent magnetization (M_r) ranges between 0.70 and 0.81 of the wire's saturation magnetization (M_s), according to[7]

$$\frac{R_c}{R_m} = \left[\frac{M_r}{M_s} \right]^{1/2} , \qquad (40)$$

also used for glass-covered wires.[14]

In order to verify by experimental means the results obtained by calculations, glass-covered amorphous $Fe_{77.5}Si_{7.5}B_{15}$ wires were prepared by the above described procedure[15] at the Institute of Technical Physics Iasi, having the diameter of the metal ranging between 3 and 22 μm and the glass cover thickness ranging between 3 and 15 μm. Magnetic measurements were performed using a fluxmeter method[21] at a maximum value of the axially applied field of 150 Oe, at a frequency of 400 Hz. All the wires that were measured present a bistable flux reversal phenomenon in low axial fields; at 1 Oe for a wire having $R_m = 7.8$ μm and $d_g = 4.5$ μm and at 50 Oe for a wire having $R_m = 1.6$ μm and $d_g = 10.4$ μm.

We must notice that M_r is about 0.95 of M_s (measured at the maximum field). The value of M_s measured by the fluxmeter method is close to the value measured with the VSM (vibrating sample magnetometer) in a 1 T magnetic field. From the ratio M_r/M_s (also called the reduced remanence) determined experimentally it results that the radius of the cylindrical inner core is about 97% of R_m, higher than the value calculated by us only from theoretical considerations (83–90 %).

The difference between these values can be attributed to a supplementary axial tensile stress induced in the preparation process of the glass-covered wire due to its continuous drawing. In order to verify this hypothesis we conducted two experiments. Thus, we determined ex-

FIG. 8. (a) Maximum value of the total axial stress in function of the glass cover thickness for three wires having almost the same radius of the metal: wire Nos. 1 (■), 2 (□), and 6 (◨) from Table I; (b) Position of the relative intersection point between σ_{rr} and σ_{zz} in function of the glass cover thickness for wire Nos. 1 (■), 2 (□), and 6 (◨).

perimentally the reduced remanence of the glass-covered amorphous wires subjected to external tensile stresses up to 500 MPa and we noticed that there was no change in the reduced remanence. Using a chemical etching technique[14] we removed the glass cover from a metallic wire having $R_m = 8.15$ μm and we determined again the reduced remanence, finding values of about 0.75, that lead to $R_c \sim 87\%$, close to the results calculated for a sample having $R_m = 7.65$ μm and $d_g = 4.75$ μm (wire No. 4 from Table I). If we apply an external tensile stress of about 250 MPa on the wire having $R_m = 8.15$ μm after the glass removal, the ratio M_r/M_s returns to its initial value of about 0.95.

These experiments allow us to consider that in the preparation process of the glass-covered amorphous wires, supplementary axial tensile stresses are induced and are added to the already existing ones. The diminishing of the total axial stress after the glass removal leads to a quite satisfactory accordance between the theoretically calculated results and the experimental ones. It is plausible that these supplementary axial tensile stresses are induced due to the mechanical drawing of the wire during its preparation process, the estimation of their values being extremely difficult by theoretical considerations.

III. CONCLUSION

We have calculated the values of the internal stresses induced on the radial, axial, and azimuthal directions during the preparation process of the glass-covered amorphous $Fe_{77.5}Si_{7.5}B_{15}$ magnetic wires. These stresses are owing to the solidification of the metal as well as to the contractions generated by the glass cover in the metal during the cooling from T_g to RT due to the difference between the thermal expansion coefficients of metal and glass. The total stresses have values of the order of 10^9 Pa that depend on the dimensions of the metallic part of the wire and of the glass cover as well as on their ratio.

The axial tensile stresses are prevalent up to $\sim 85\%$ of R_m, from where the radial stresses become prevalent until $\sim 88\%$ of R_m and then, up to $r = R_m$, the compressive axial and azimuthal stress components are prevalent. By taking into account the high positive magnetostriction of the FeSiB alloy, the following easy axes distribution results in these wires: up to $\sim 85\%$ of R_m there is a region having the easy axis on the longitudinal direction (z) of the wire and from here until $r = R_m$ there is a region having radial easy axes of magnetization. We can associate to this easy axes distribution a magnetic domain structure consisting of a cylindrical inner core which is axially magnetized and of an outer shell which is radially magnetized.

The calculated value of the cylindrical inner core leads to a value of the ratio M_r/M_s (the reduced remanence) of about 0.75–0.80, depending on the dimensional characteristics of the wire. But, the experimentally determined reduced remanence is approximately 0.95. The experimentally established dependence of the reduced remanence on the value of the external tensile stresses for wires after the glass removal shows that in the preparation process of the glass-covered amorphous wires a supplementary axial tensile stress appears due to the mechanical drawing of the wire. The value of this stress component depends on the dimensional characteristics of the wire and it can be estimated as being about 250–600 MPa. The high values of the reduced remanence in highly magnetostrictive glass covered amorphous wires opens up a larger field of sensing applications for these wires as compared to that of the wires without a glass cover produced by the in-water quenching technique.

[1]P. T. Squire, D. Atkinson, M. R. J. Gibbs, and S. Atalay, J. Magn. Magn. Mater. **132**, 10 (1994).

[2]M. Vázquez, C. Gomez-Polo, D. X. Chen, and A. Hernando, IEEE Trans. Magn. **30**, 907 (1994).

[3]K. Mohri, K. Kawashima, T. Kohzawa, and H. Yoshida, IEEE Trans. Magn. **29**, 1245 (1993).

[4]I. Ohnaka, T. Fukusako, and T. Daido, J. Jpn. Inst. Metall. **45**, 751 (1981).

[5]T. Masumoto, A. Inoue, M. Hagiwara, U.S. Patent No. 4 523 626 (1985).

[6]M. Vázquez, C. Gomez-Polo, and D. X. Chen, IEEE Trans. Magn. **28**, 3147 (1992).

[7]A. M. Severino, C. Gomez-Polo, P. Marin, and M. Vázquez, J. Magn. Magn. Mater. **103**, 117 (1992).

[8]F. B. Humphrey, K. Mohri, J. Yamasaki, H. Kawamura, R. Malmhall, and I. Ogasawara, in *Magnetic Properties of Amorphous Metals*, edited by A. Hernando *et al.* (North-Holland, Amsterdam, 1987), p. 110.

[9]C. Gomez-Polo, M. Vázquez, and D. X. Chen, Appl. Phys. Lett. **62**, 108 (1993).

[10]J. Liu, R. Malmhall, L. Arnberg, and S. J. Savage, J. Appl. Phys. **67**, 4238 (1990).

[11]V. Madurga and A. Hernando, J. Phys. Condens. Matter **2**, 2127 (1990).

[12]J. L. Costa and K. V. Rao, in *Proceedings of the 5th International Conference on Physics of Magnetic Materials,* edited by W. Gorzkowski *et al.* (World Scientific, Singapore, 1991), p. 279.

[13]J. Velázquez, M. Vázquez, A. Hernando, H. T. Savage, and M. Wun-Fogle, J. Appl. Phys. **70**, 6525 (1991).

[14]H. Chiriac, Gh. Pop, F. Barariu, and M. Vázquez, J. Appl. Phys. **75**, 6949 (1994).

[15]M. Hagiwara and A. Inoue, in *Production Techniques of Alloy Wires by Rapid Solidification in Rapidly Solidified Alloys,* edited by H. H. Liebermann (Marcel Dekker, New York, 1993), p. 141.

[16]E. R. G. Eckert, *Introduction to Heat and Mass Transfer* (McGraw-Hill, New York, 1963), p. 22.

[17]B. A. Bosley and J. H. Weiner, *Theory of Thermal Stresses* (Wiley, New York, 1960), p. 290.

[18]L. Landau and E. Lifchitz, *Physique Théorique, Tome 7–Théorie de l'elasticité* (Mir, Moscou, 1990), pp. 26–31.

[19]V. Madurga, J. L. Costa, A. Inoue, and K. V. Rao, J. Appl. Phys. **68**, 1164 (1990).

[20]F. Kinoshita, IEEE Trans. Magn. **26**, 1786 (1990).

[21]K. Mandal and S. K. Ghatak, J. Magn. Magn. Mater. **118**, 315 (1993).